Morphology and Phase Diagram of Complex Block Copolymers: ABC Star Triblock Copolymers

Ping Tang, Feng Qiu,* Hongdong Zhang, and Yuliang Yang

Department of Macromolecular Science,The Key Laboratory of Molecular Engineering of Polymers, Ministry of Education, Fudan University, Shanghai 200433, China

Received: December 18, 2003; In Final Form: April 13, 2004

Microphases and triangle phase diagrams of ABC star triblock copolymers are investigated on the basis of a real-space implementation of the self-consistent field theory (SCFT) for polymers. For the sake of numerical tractability, the calculations are carried out in two dimensions (2D). Nine stable microphases are uncovered, including hexagonal lattice, core−shell hexagonal lattice, lamellae, and lamellae with beads at the interface as well as a variety of complex morphologies that are absent in linear ABC triblocks, such as a "three-color" hexagonal honeycomb phase, knitting pattern, octagon−octagon−tetragon phase, lamellar phase with alternating beads, and decagon−hexagon−tetragon phase. We have found that when the volume fractions of the three species are comparable the star architecture of the polymer chain is a strong topological constraint that regulates the geometry of the microphases formed. However, when at least one of the volume fractions of the three species is low, the influence of the star architecture on the morphology is not significant. Our calculations reasonably agree with previous theoretical and experimental results and can be used to guide the design of novel microstructures involving star triblock copolymers.

I. Introduction

Block copolymers are produced by linking two or more chemically different homopolymers into a single macromolecule. The chemically distinct blocks normally undergo microphase separation, creating intricate morphologies that have applications ranging from thermoplastic elastomers to adhesives, coatings, and templates for nanocomposites.[1,2] For the simplest AB diblock copolymer, it has been recognized that, depending on the composition and the chemical interaction (usually described by the Flory−Huggins interaction parameter) between the two species, only four stable microphases—spheres, cylinders, gyroids, and lamellae—exist under equilibrium conditions. However, as the number of distinct blocks is increased from two to three, say, ABC triblocks, both the complexity and variety of self-assembled structures are significantly increased.[3−6] For triblock copolymers, the microphases depend not only on the composition and interaction energies between distinct blocks but also on their particular molecular architectures. For example, the phase behavior of ABC linear triblock copolymers crucially depends on the sequence of the blocks in the chain (i.e., whether it is sequenced A−B−C, B−C−A, or C−A−B).[7−9] Indeed, a range of characterization experiments have been applied to various sample linear ABC triblock copolymers and have provided detailed evidence of the profound effects of block sequencing on their equilibrium morphology.[3,7,9]

More interestingly, instead of being consecutively joined to form a linear triblock chain, the A, B, and C blocks may also form a star-shaped copolymer by joining one of the ends of each block together at a center core. Compared to linear block copolymers, an additional entropic effect due to the junction constraint of the center cores arises in the star block copolymers even in the disordered state. While in ordered states, the existence of the cores becomes a strong topological constraint that regulates the formation of various geometric structures. In contrast to linear triblocks, the experimental study of the phase behavior of ABC star triblocks is limited by difficulties in their synthesis and exact characterization of the structure.[10−15]

Only a few theoretical approaches, such as Monte Carlo simulations[16] and the density functional method,[17,18] were used to investigate the microphase formation of ABC star triblock copolymers. However, because of the difficulties of numerical computation, only a few points in the parameter space are touched. Therefore, a systematic investigation of how the phase behavior is related to the star architecture is still desired. In this paper, we use a combinatorial screening method, which was recently proposed by Drolet and Fredrickson,[19,20] to search for possible new microphases formed in ABC star triblocks. The screening method involves the direct implementation of the self-consistent field theory (SCFT) for polymers in real space in an adaptive arbitrary cell. In previous work,[21] we have used this method to predict the microphases and triangle phase diagrams for linear ABC triblock copolymers. We now expand it to search the equilibrium microphases of ABC star triblock copolymer melts. On the basis of these microphases, three-component triangle phase diagrams in the entire range of the copolymer composition are constructed, and the influence of the composition, interaction parameters, and their relative strengths on microphase formation is investigated.

II. Theoretical Method

We consider a system with volume V of n star block copolymers each having A, B, and C arms joined together at a center core. The total degree of polymerization of the star block is N, and the A, B, and C blocks consist of $f_A N$, $f_B N$, and $f_C N$ monomers, respectively. Each star polymer is parametrized with the variable s, which increases along each arm. The core of the

* To whom all correspondence should be addressed. E-mail: fengqiu@fudan.edu.cn.

10.1021/jp037911q CCC: $27.50
Published on Web 05/22/2004

star corresponds to $s = 0$. Along the A arm, s increases from 0 at the core to $f_A N$ at the outer end. The B and C arms are parametrized similarly. With these definitions, the polymer segment probability distribution functions $q_K(\mathbf{r}, s)$ and $q_K^+(\mathbf{r}, s)$ for species K satisfy the modified diffusion equations:[22,23]

$$\frac{\partial q_K(\mathbf{r}, s)}{\partial s} = \frac{a^2}{6}\nabla^2 q_K(\mathbf{r}, s) - \omega_K(\mathbf{r})\, q_K(\mathbf{r}, s)$$

$$\frac{\partial q_K^+(\mathbf{r}, s)}{\partial s} = -\frac{a^2}{6}\nabla^2 q_K^+(\mathbf{r}, s) + \omega_K(\mathbf{r}) q_K^+(\mathbf{r}, s) \qquad (1)$$

where a is the Kuhn length of the polymer segment, $\omega_K(\mathbf{r})$ is the self-consistent field for species K, and $0 < s < f_K N$. The initial conditions are $q_K(\mathbf{r}, 0) = q_L^+(\mathbf{r}, 0)\, q_M^+(\mathbf{r}, 0)$ and $q_K^+(\mathbf{r}, f_K N) = 1$, where (KLM) $\in$ {(ABC), (BCA), (CAB)}. Note that one must solve for $q_K^+(\mathbf{r}, s)$ prior to solving for $q_K(\mathbf{r}, s)$. Accordingly, the partition function of a single chain subject to the mean field $\omega_K(\mathbf{r})$ can be written as $Q = \int d\mathbf{r}\, q_K(\mathbf{r}, s)\, q_K^+(\mathbf{r}, s)$ in terms of $q_K(\mathbf{r}, s)$ and $q_K^+(\mathbf{r}, s)$. We note that Q is independent of the contour length parameter of a chain, s.

With the above description, the free energy of the system is given by

$$\frac{F}{nk_BT} = -\ln\left(\frac{Q}{V}\right) + \left(\frac{N}{V}\right)\int d\mathbf{r}[\chi_{AB}\phi_A\phi_B + \chi_{BC}\phi_B\phi_C + \chi_{AC}\phi_A\phi_C - \omega_A\phi_A - \omega_B\phi_B - \omega_C\phi_C - \xi(1 - \phi_A - \phi_B - \phi_C)] \qquad (2)$$

where ϕ_A, ϕ_B, and ϕ_C are the monomer density field normalized by the local volume fractions of A, B, and C, respectively. χ_{AB}, χ_{BC}, and χ_{AC} are Flory−Huggins parameters between different species. $\xi(\mathbf{r})$ is the potential field that ensures the incompressibility of the system, also known as a Lagrange multiplier. Minimizing the free energy in eq 2 with respect to ϕ_A, ϕ_B, ϕ_C, ω_A, ω_B, ω_C, and ξ leads to the following self-consistent field equations that describe the equilibrium morphology:

$$\omega_A(\mathbf{r}) = \chi_{AB}\phi_B(\mathbf{r}) + \chi_{AC}\phi_C(\mathbf{r}) + \xi(\mathbf{r}) \qquad (3)$$

$$\omega_B(\mathbf{r}) = \chi_{AB}\phi_A(\mathbf{r}) + \chi_{BC}\phi_C(\mathbf{r}) + \xi(\mathbf{r}) \qquad (4)$$

$$\omega_C(\mathbf{r}) = \chi_{AC}\phi_A(\mathbf{r}) + \chi_{BC}\phi_B(\mathbf{r}) + \xi(\mathbf{r}) \qquad (5)$$

$$\phi_A(\mathbf{r}) + \phi_B(\mathbf{r}) + \phi_C(\mathbf{r}) = 1 \qquad (6)$$

$$\phi_A(\mathbf{r}) = \frac{V}{NQ}\int_0^{f_A N} ds q_A(\mathbf{r}, s)\, q_A^+(\mathbf{r}, s) \qquad (7)$$

$$\phi_B(\mathbf{r}) = \frac{V}{NQ}\int_0^{f_B N} ds q_B(\mathbf{r}, s)\, q_B^+(\mathbf{r}, s) \qquad (8)$$

$$\phi_C(\mathbf{r}) = \frac{V}{NQ}\int_0^{f_C N} ds q_C(\mathbf{r}, s)\, q_C^+(\mathbf{r}, s) \qquad (9)$$

We solve eqs 3−9 directly in real space by using a combinatorial screening algorithm proposed by Drolet and Fredrickson.[19,20] The algorithm consists of randomly generating the initial values of the fields $\omega_K(\mathbf{r})$. Using a Crank−Nicholson scheme and the alternating-direct implicit (ADI) method,[24] we then integrate the diffusion equations to obtain q and q^+ for $0 \le s \le f_K N$. Next, the right-hand sides of eqs 7−9 are evaluated to obtain new expression values for the volume fractions of blocks A, B, and C. $\xi(\mathbf{r})$ is then chosen to be

$$\xi(\mathbf{r}) = \lambda[1 - \phi_A(\mathbf{r}) - \phi_B(\mathbf{r}) - \phi_C(\mathbf{r})] \qquad (10)$$

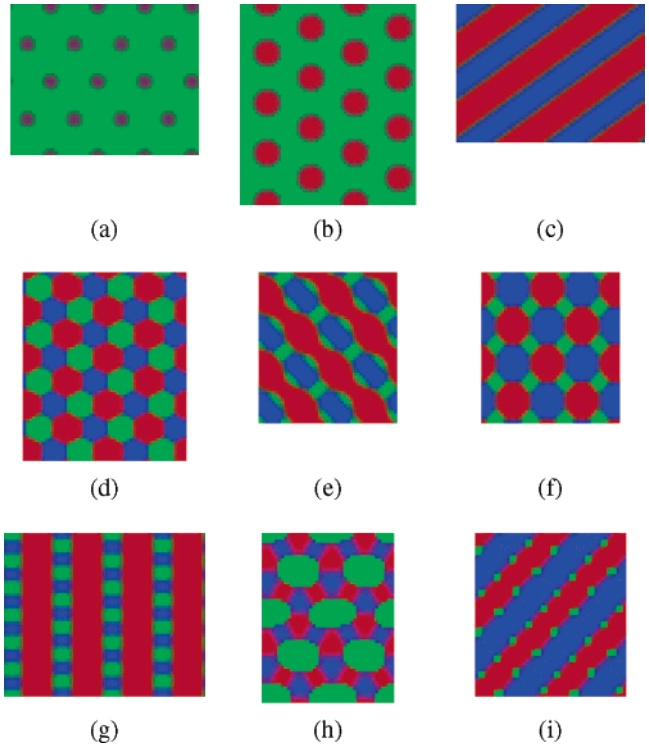

Figure 1. Schematics of the 2D ordered microphases for ABC star triblock copolymers. (a) Hexagonal lattice phase (HEX), (b) core−shell hexagonal lattice phase (CSH); (c) three-color lamellae phase (LAM_3), (d) three-color hexagonal honeycomb phase (HEX_3); (e) knitting pattern (KP), (f) octagon−octagon−tetragon phase (OOT), (g) lamellae phase with alternating beads (LAM + BD), (h) decagon−hexagon−tetragon phase (DEHT), and (i) lamellae phase with beads at the interface (LAM + BD-I).

where λ is large enough to enforce the incompressibility of the system (i.e., eq 6) and the resulting density profiles and free energies should be independent of its particular value. Finally, the potential fields $\omega_K(\mathbf{r})$ and $\xi(\mathbf{r})$ are updated using eqs 3−5 and 10 by means of a linear mixing of new and old solutions. These steps are repeated until the relative free-energy changes at each iteration are reduced to 10^{-4}. To avoid the real-space method becoming trapped in a metastable state, random noise is added to the fields to disturb the state formed in the iteration. In addition, we also minimize the free energy with respect to the system size because it has been pointed out that the box size can influence the morphology.[17] Each minimization is repeated several times and examined using different initial conditions. In this way, by varying the composition and the interaction parameters systematically, we can obtain not only the typical microphases but also the phase diagram.

For the sake of numerical tractability, the implementation of the SCF equations is carried out on a 2D $L_x \times L_y$ lattice with periodic boundary conditions. The chain length of the polymers is fixed to $N = 100$. The lattice spacings are chosen to be $dx = dy = a$, where a is the Kuhn length of the polymer segment. Because the radius of gyration of the polymer chain satisfies $R_g^2 = Na^2/6$ and typically the microstructure period $D \approx 2R_g$, the lattice spacings dx and dy are $\sim 0.1D$. The typical lattice size of L_x and L_y is $\sim 10R_g$.

III. Results and Discussion

Figure 1 shows all of the 2D microphases that we have obtained for ABC star triblock copolymers. The morphology is represented in the form of density plots with intensity proportional to the local composition (volume fraction) of the triblock

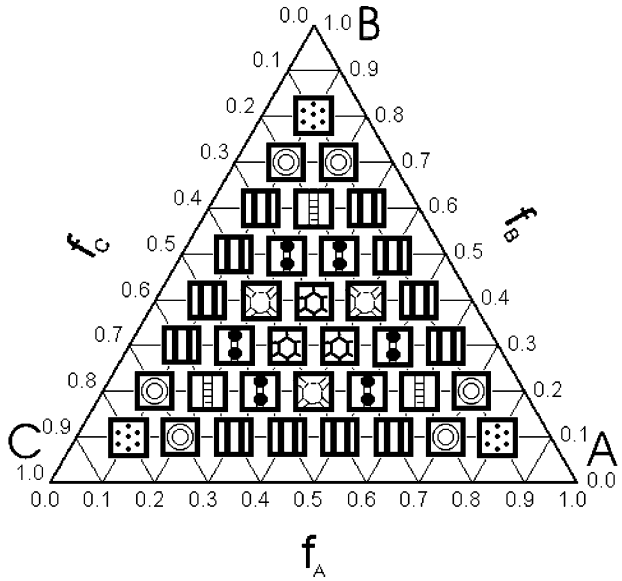

Figure 2. Phase diagram for $\chi_{AB}N = \chi_{BC}N = \chi_{AC}N = 35$. Hexagonal lattice phase (HEX); core−shell hexagonal lattice phase (CSH); three-color lamellae phase (LAM_3); lamellae phase with alternating beads (LAM + BD); knitting pattern (KP); octagon−octagon−tetragon phase (OOT); three-color hexagonal honeycomb phase (HEX_3).

copolymers. Three different colors—blue, green, and red , respectively—are assigned to A, B, and C blocks. For a clear presentation of the final pattern, the linear dimensions of the unit cell are replicated two times in each direction. Nine microphases are observed: hexagonal lattice (HEX), core−shell hexagonal lattice (CSH), three-color lamellae (LAM_3), three-color hexagonal honeycomb (HEX_3), knitting pattern (KP), octagon−octagon−tetragon (OOT), lamellae with alternating beads inside (LAM + BD), decagon−hexagon−tetragon (DEHT), and alternating lamellae phases with beads at the interface (LAM + BD-I). It is interesting that all of the polygonal structures that we obtained (HEX_3, OOT, DEHT) are even-numbered, which agrees with the Monte Carlo simulations by Gemma et al.[16]

A. Symmetric Interaction Parameters ($\chi_{AB} = \chi_{BC} = \chi_{AC}$). We first discuss the case with symmetric interaction parameters among three species, and hence the influence of copolymer compositions on the morphology is highlighted. The three-component triangle phase diagram with Flory−Huggins parameters $\chi_{AB}N = \chi_{BC}N = \chi_{AC}N = 35$ is shown in Figure 2. The increment of volume fractions f_A, f_B, and f_C in the phase diagram is 0.1. At each grid point, the equilibrium morphologies are obtained in the way described in section II and represented by schematic symbols.

In Figure 2, the triangle diagram clearly shows A−B, B−C, and A−C permutation symmetry. Therefore, switching the sequences of blocks A and B (ABC → BAC), B and C (ABC → ACB), and A and C (ABC → CBA) does not alter the phase symmetry for the system with symmetric interactions between the three distinct blocks. This feature arises from the special molecular architecture of the star triblocks. On the contrary, for linear ABC triblock copolymers, the morphologies and hence the phase diagram are crucially influenced by the sequence of blocks.[3,7−9,21]

Near the three edges (AB, BC, and AC) of the triangle diagram in Figure 2, where the volume fraction of one of the blocks (f_C, f_A, and f_B) is no more than 0.1, three types of microphases (i.e., hexagonal lattice (HEX), core−shell hexagonal (CSH), and three-color lamellae (LAM_3), as shown in Figure 1a−c, respectively) are found. It is interesting that these three microphases are also observed in a similar region for ABC linear triblock copolymers. Therefore, when one of the blocks is relatively short, the influence of the star architecture on the morphology is not significant.

TABLE 1: Saddle Point Free Energy of Different Phases for Symmetric Interactions

composition ($f_A/f_B/f_C$)	morphology	saddle point free energy	free energies with strong segregation (F_{min}/k_bT)
0.8/0.1/0.1	HEX	5.90785	
0.7/0.2/0.1	CSH	7.02661	
0.6/0.3/0.1	LAM_3	7.29861	
0.6/0.2/0.2	LAM+BD	8.41801	7.5757
0.5/0.3/0.2	KP	8.90715	
0.4/0.4/0.2	OOT	8.94645	7.6064
0.4/0.3/0.3	HEX_3	9.38304	7.6403

In the center region of the phase diagram, where the volume fractions of the three species are comparable, the situation is completely different. Three types of novel complex microphases—the three-color hexagonal honeycomb phase (HEX_3), knitting pattern (KP), and octagon−octagon−tetragon phase (OOT), whose structures are shown in Figure 1d−f, respectively—are observed. These phases, however, are absent in linear ABC triblocks. Among these complex phases, a perfect HEX_3 phase (Figure 1d) is formed at nearly equal volume fractions of the three species (symmetric triblocks, $f_A \approx f_B \approx f_C$). The same morphology has also been predicted in three-arm star triblocks with equal volume fractions by Bohbot-Raviv and Wang in terms of minimizing an approximate free-energy functional,[17] recently by He et al. using dynamic density functional theory,[18] and by Dotera and Hatano using Monte Carlo simulations.[16,25] Unfortunately, to date, experimental evidence has not yet been found to confirm this structure, mainly because of difficulties in the synthesis of such star triblock copolymers with equal interaction energies among the three species. In fact, as we will see later, the HEX_3 phase disappears when the interaction parameters become asymmetric. When the volume fraction of one of the blocks, say, A, is $f_A = 0.2$ and the other two blocks have equal composition, $f_B = f_C = 0.4$, an octagon−octagon−tetragon phase (OOT) is found. In this case, the longer blocks B and C form octagonal domains, and shorter A blocks form tetragonal domains. Gemma et al. also predicted similar morphology with the same composition in their Monte Carlo simulations.[16] Another interesting microphase, which is absent in linear ABC triblock copolymers and is referred to as lamellae with alternating beads inside (LAM + BD), shown in Figure 1g, occurs when $f_A(f_B, f_C) = 0.2$, $f_B(f_C, f_A) = 0.6$, and $f_C(f_A, f_B) = 0.2$.

In Figure 2, when $f_A = f_C$, as the volume fraction f_B increases, the ordered microphases change from LAM_3 to OOT, to HEX_3, to KP, to LAM + BD, to CSH, and finally to HEX phases. However, when χN is large enough (e.g., $\chi N \geq 80$), alternating lamellar structure with beads formed by the shorter blocks regularly located at the interface is found in the region between LAM_3 and OOT. A similar morphology transformation due to increasing χN was also predicted by Gemma et al.[16]

To compare the energetic closeness of these microphases, we have listed (Table 1) the minimized free energies (saddle point free energies) for the typical phases of star triblock copolymers with symmetric interaction parameters. We see that the saddle point free energy is higher as the volume fractions of the three species (f_A, f_B, f_C) become more comparable. The

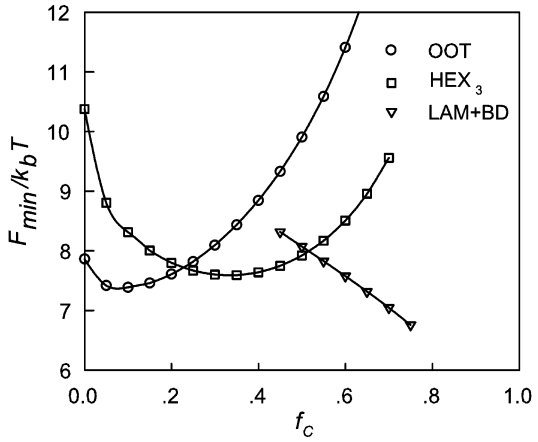

Figure 3. Plot of the free energies of OOT, HEX_3 and LAM + BD phases vs f_C ($f_A = f_B$, $\chi_{AB}N = \chi_{BC}N = \chi_{AC}N = 35$) using strong-segregation theory.

reason is that the interfacial areas (in a unit volume) between the incompatible components are larger for triblocks with comparable volume fractions of the three species. However, we note that the saddle point free energies of the KP and OOT phases are very close, suggesting that these two phases compete for stability with each other in their respective stable regions. Therefore, it is possible experimentally to observe a (metastable) KP (OOT) phase in the stable region of the OOT (KP) phase that is predicted by the present phase diagram.

In Table 1, we also list the minimized free energy for the LAM + BD, OOT, and HEX_3 phases that is predicted by the strong-segregation theory (SST) for star triblock copolymers. For details of the calculation, see ref 16. The reason that we choose only these three phases for the SST calculation is the following. The SST assumes that different blocks are strongly stretched and completely separated except for a narrow region about the interfaces, which is believed to be accurate in the $\chi N \rightarrow \infty$ limit. Furthermore, the present form of SST can treat microphases with only simple geometrical structures. Our SCF calculation, however, is performed in an intermediate χN regime. Therefore, we observe a complex structure—the KP phase and various microphases with mixed blocks, such as the HEX, CSH, and LAM_3 structures. An accurate calculation of the free energy for such phases in the frame of SST is absent at present. Even for the microphases that can be treated by the SST, the predicted free energy is always lower than that calculated by the SCFT. Nevertheless, as shown in Figure 3, if one keeps $f_A = f_B$ and increases f_C, starting from the OOT phase, then the stable phases predicted by the SST follow the order OOT, HEX_3, and LAM + BD, which is in agreement with the SCF calculation (Figure 2).

B. Asymmetric Interaction Parameters. In this section, we focus on the influence of the asymmetry of the interaction parameters among the three species on the phase behavior of star triblock copolymers. We investigate a typical case in which the interactions between blocks A and C are less unfavorable than that between the AB and BC pairs. Therefore, the system tends to form morphologies that can avoid contacts between blocks A (B) and B (C), whereas the three domains have to adjoin at the core because of the star architecture. Figure 4 shows an example phase diagram for $\chi_{AB}N = 72$, $\chi_{BC}N = 72$, and $\chi_{AC}N = 22$. Obviously, the permutation symmetry among A, B, and C blocks in the symmetric case is reduced to that only between blocks A and C because of the interaction parameters that we have assumed. Near the AC edge (where f_B is no more than 0.1), when the compositions of the A and C blocks are

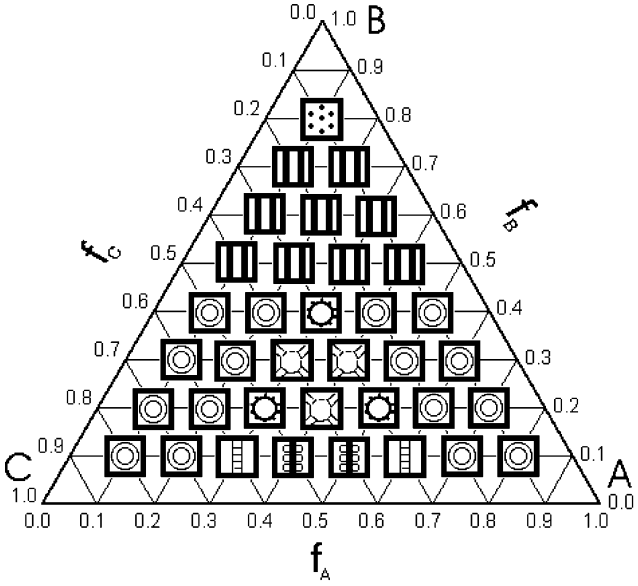

Figure 4. Phase diagram for $\chi_{AB}N = 72$, $\chi_{BC}N = 72$, and $\chi_{AC}N = 22$. Core−shell hexagonal lattice phase (CSH); lamellae phase with alternating beads (LAM + BD); lamellae phase with beads at the interface (LAM + BD-I); decagon−hexagon−tetragon phase (DEHT); octagon−octagon−tetragon phase (OOT); three-color lamellae phase (LAM_3); hexagonal lattice (HEX).

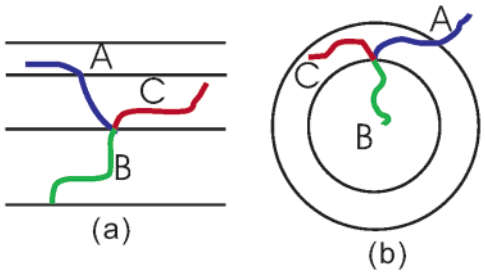

Figure 5. Schematic representation of the microstructures of LAM_3 and CSH.

comparable, the system tends to form a microphase with alternating A and C lamellae with circular beads of minority B blocks located at the A/C interfaces (LAM + BD-I), whose structure is schematically shown in Figure 1i. It is interesting that a similar micorphase was also observed by Gemma et al. with the composition of (A:B:C/1:1:0.17 ≈ 0.33) in Monte Carlo simulations but with symmetric interaction parameters.[16] When B blocks are the majority species ($f_B \geq 0.5$), then the LAM_3 phase is formed because of slightly unfavorable contacts between the A and C blocks. In this phase, the cores of star triblocks lie on the B/C interfaces, and the A blocks have to penetrate the C domains. Thus, the A blocks have to mix partially with C blocks to meet the requirement of the star architecture, as schematically shown in Figure 5a.

Near the AB and BC edges, where $f_B < 0.45$, $f_C < 0.25$, or $f_A < 0.25$, CSH structures are formed, with B blocks forming the cores, C (A) blocks forming the shells, and A (C) blocks being the matrix (as shown in Figure 5b) to reduce the interfacial energy between the B (A) and C (B) blocks. Furthermore, the less unfavorable interaction between the A and C blocks makes it possible for the two blocks to mix partially to satisfy the requirement that three blocks have to join at the core of the star. It is interesting to compare this predicted phase with the experimental findings by Thomas et al.,[26] who studied star triblocks of polystyrene (PS), polyisoprene (PI), and poly(methyl methacrylate) (PMMA) in which PS and PMMA are weakly

TABLE 2: Saddle Point Free Energy of Different Phases for Asymmetric Interactions

composition ($f_A/f_B/f_C$)	morphology	saddle point free energy
0.1/0.8/0.1	HEX	7.66936
0.4/0.5/0.1	LAM_3	8.32829
0.6/0.1/0.3	LAM + BD	9.22091
0.5/0.1/0.4	LAM + BD-I	9.50425
0.4/0.4/0.2	CSH	9.67021
0.5/0.2/0.3	DEHT	10.12300
0.4/0.3/0.3	OOT	10.1507

incompatible but show a strong incompatibility toward PI. It was found that CSH morphology was observed with the compositions of PS−PI−PMMA (0.21/0.23/0.56 and 0.20/0.21/0.59), which is qualitatively in agreement with our theoretical calculation in Figure 4. Finally, we note that in the case of equal interaction parameters in Figure 2 a perfect three-color hexagonal honeycomb phase (HEX_3) occurs at nearly equal volume fractions of the three components. With asymmetric interaction parameters in Figure 4, however, octagon−octagon−tetragon (OOT) and decagon−hexagon−tetragon (DEHT) structures are found instead for the same composition. We speculate that this might be the reason that the hexagonal honeycomb phase has never been observed in experiments. Indeed, it is difficult to synthesize an exactly symmetric ABC star triblock copolymer, especially with equal interaction energies. The octagon−octagon−tetragon (OOT) phase similar to our calculation but with the polygons bent into arcs was found in a recent experiment by Hasegawa et al.,[27] who studied the microphases of star polystyrene (PS)−polyisoprene (PI)−poly(dimethylsiloxane) (PDMS) with the volume fraction of 1:1:1 by using energy-filtering TEM and 3D electron tomography. They claimed that the OOT structure is due to the asymmetric interactions among the three distinct blocks, where both PDMS and PI show stronger unfavorable interactions toward PS, in contrast to the relatively weak incompatibility between PI and PDMS.

The minimized free energies of typical phases with asymmetric interaction parameters are listed in Table 2. As is observed in the case with symmetric interactions, in general the phases with more comparable volume fractions of the three components have higher free energy. The saddle point free energies for the phases of OOT and DEHT are extremely close to each other, suggesting that these phases compete to exist and thus might be experimentally observed in the same region of the phase diagram. It should be noted that the SST is inapplicable in the regime of the asymmetric interaction parameters that we used because one of the interaction parameters, $\chi_{AC}N = 22$, is far away from the strong-segregation limit.

IV. Conclusions

Using a combinatorial screening method based on the SCFT for polymers, we have investigated the self-assembled structures of ABC star triblock copolymer melts. Nine ordered, stable microphases in 2D are observed, including a hexagonal phase, core−shell hexagonal phase, lamellar phase, and alternating lamellar phase with beads at the interface as well as complex ordered structures such as a three-color hexagonal honeycomb phase, knitting pattern, octagon−octagon−tetragon phase, lamellae with alternating beads inside, and decagon−hexagon−tetragon phase. By systematically varying the composition, the triangle phase diagrams are constructed for ABC star triblocks both with symmetric and asymmetric interaction parameters among the three species. It is found that when the volume fractions of the three blocks are comparable the star architecture plays a profound role in the complex microphase formation. To meet the requirements of star architecture, various complex structures including knitting pattern, lamellae with alternating beads inside, and even-numbered polygonal phases such as three-color hexagonal honeycomb, octagon−octagon−tetragon, and decagon−hexagon−tetragon phases, which are absent in linear ABC triblocks, are formed. However, when one of the blocks is relatively short with χN values that are not very large, the star architecture is less important; therefore, the phase behavior is similar to that of linear triblocks. However, this feature will disappear when χN reaches larger values or the interaction parameters become asymmetric. In general, the triangle phase diagrams we present, as a first step, may be used as a guide for designing possible ordered structures involving star ABC triblock copolymers.

Acknowledgment. We gratefully acknowledge financial support from the Special Funds for Major State Basic Research Projects (G1999064800) and the NSF of China (grant nos. 20104002, 20234010, 20374016, 20304002, and the Grant for the Excellent Research Group). F.Q. acknowledges the Ministry of Education of China (FANEDD 200225) and the STCSM (grant no. 02QE14010).

References and Notes

(1) Park, M.; Harrison, C.; Chaikin, P. M.; Register, R. A.; Adamson, D. H. *Science* **1997**, *276*, 1401.
(2) Bates, F. S.; Fredrickson, G. H. *Phys. Today* **1999**, *52*, 32.
(3) Mogi, Y.; Mori, K.; Matsushita, Y.; Noda, I. *Macromolecules* **1992**, *25*, 5412.
(4) Stadler, R.; Auschra, C.; Beckmann, J.; Krappe, U.; Voigtmartin, I.; Leibler, L. *Macromolecules* **1995**, *28*, 3080.
(5) Breiner, U.; Krappe, U.; Thomas, E. L.; Stadler, R. *Macromolecules* **1998**, *31*, 135.
(6) Goldacker, T.; Abetz, V. *Macromolecules* **1999**, *32*, 5165.
(7) Mogi, Y.; Kotsuji, H.; Kaneko, Y.; Mori, K.; Matsushita, Y.; Noda, I. *Macromolecules* **1992**, *25*, 5408.
(8) Zheng W.; Wang, Z.-G. *Macromolecules* **1995**, *28*, 7215.
(9) Gido, S. P.; Schwark, D. W.; Thomas, E. L.; Goncalves, M. *Macromolecules* **1993**, *26*, 2636.
(10) Iatrou, H.; Hadjichristidis, N. *Macromolecules* **1992**, *25*, 4649.
(11) Fujimoto, T.; Zhang, H. M.; Kazama, T.; Isono, Y.; Hasegawa, H.; Hashimoto, T. *Polymer* **1992**, *33*, 2208.
(12) Huckstadt, H.; Abetz V.; Stadler, R. *Macromol. Rapid Commun.* **1996**, *17*, 599.
(13) Sioula, S.; Tselikas, Y.; Hadjichristidis, N. *Macromolecules* **1997**, *30*, 1518.
(14) Lambert, O.; Reutenauer, S.; Hurtrez, G.; Riess G.; Dumas, P. *Polym. Bull.* **1998**, *40*, 143.
(15) Huckstadt, H.; Gopfert, A.; Abetz, V. *Macromol. Chem. Phys.* **2000**, *201*, 296.
(16) Gemma, T.; Hatano, A.; Dotera, T. *Macromolecules* **2002**, *35*, 3225.
(17) Bohbot-Raviv, Y.; Wang, Z.-G. *Phys. Rev. Lett.* **2000**, *85*, 3428.
(18) He, X. H.; Huang, L.; Liang, H. J.; Pan, C. Y. *J. Chem. Phys.* **2003**, *118*, 9861.
(19) Drolet, F.; Fredrickson, G. H. *Macromolecules* **2001**, *34*, 5317.
(20) Drolet, F. Fredrickson, G. H. *Phys. Rev. Lett.* **1999**, *83*, 4317.
(21) Tang, P.; Qiu, F.; Zhang H. D.; Yang, Y. L. *Phys. Rev. E* **2004**, *69*, 031803.
(22) Helfand, E. *J. Chem. Phys.* **1975**, *62*, 999.
(23) Edwards, S. F. *Proc. Phys. Soc.* **1965**, *85*, 613.
(24) Press, W. H.; Flannery, B. P.; Teukolsky, S. A.; Vetterling, W. T. *Numerical Recipes*; Cambridge University Press: Cambridge, England, 1989.
(25) Dotera, T.; Hatano, A. *J. Chem. Phys.* **1996**, *105*, 8413.
(26) Sioula, S.; Hadjichristidis, N.; Thomas, E. L. *Macromolecules* **1998**, *31*, 8429.
(27) Yamauchi, K.; Takahashi, K.; Hasegawa, H.; Iatrou, H.; Hadjichristidis, N.; Kaneko, T.; Nishikawa, Y.; Jinnai, H.; Matsui, T.; Nishioka, H.; Shimizu, M.; Furukawa, H. *Macromolecules* **2003**, *36*, 6962.